ACS OMEGA

http://pubs.acs.org/journal/acsodf

Article

Small Molecules Targeting SARS-CoV-2 Spike Glycoprotein Receptor-Binding Domain

Yoel Rodríguez,* Scarlet Martínez Cardoze, Onyinyechi W. Obineche, Claudia Melo, Ashanna Persaud, and José A. Fernández Romero

Cite This: *ACS Omega* 2022, 7, 28779−28789

Read Online

ACCESS | Metrics & More | Article Recommendations | Supporting Information

ABSTRACT: The severe acute respiratory syndrome coronavirus 2 (SARS-CoV-2) has caused the coronavirus disease 2019 (COVID-19) pandemic. Several variants of SARS-CoV-2 have emerged worldwide. These variants show different transmissibility infectivity due to mutations in the viral spike (S) glycoprotein that interacts with the human angiotensin-converting enzyme 2 (hACE2) receptor and facilitates viral entry into target cells. Despite the effective SARS-CoV-2 vaccines, we still need to identify selective antivirals, and the S glycoprotein is a key target to neutralize the virus. We hypothesize that small molecules could disrupt the interaction of S glycoprotein with hACE2 and inhibit viral entry. We analyzed the S glycoprotein-hACE2 complex structure (PDB: 7DF4) and created models for different viral variants using visual molecular dynamics (VMD) and molecular operating environment (MOE) programs. Moreover, we started the hits search by performing structure-based molecular docking virtual screening of commercially available small molecules against S glycoprotein models using OEDocking FRED-4.0.0.0 software. The FRED-4.0.0.0 Chemguass4 scoring function was used to rank the small molecules based on their affinities. The best candidate compounds were purchased and tested using a standard SARS-CoV-2 pseudotyped cell-based bioassay to investigate their antiviral activity. Three of these compounds, alone or in combination, showed antiviral selectivity. These small molecules may lead to an effective antiviral treatment or serve as probes to better understand the biology of SARS-CoV-2.

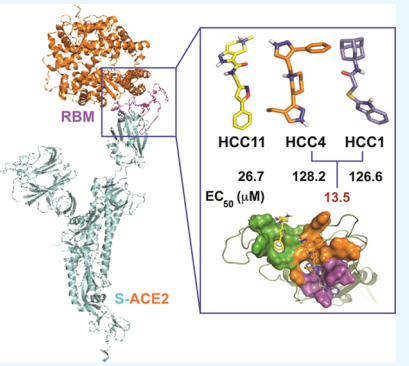

1. INTRODUCTION

On December 31, 2019, the world woke up to the news of an emerging acute respiratory viral infection in Wuhan, China. The new virus named severe acute respiratory syndrome coronavirus 2 (SARS-CoV-2) has caused the coronavirus disease 2019 (COVID-19) pandemic. SARS-CoV-2 has now (as of December 19, 2021) spread to over 211 countries resulting in over 273 million cases, and 5.3 million deaths have been reported globally.[1] A pandemic of this magnitude requires a rapid response, including developing vaccines that we have seen quickly introduced and approved by federal agencies and broad-spectrum and highly effective therapeutics. Unfortunately, we have not seen many of the last approved for use in humans, which still represents a significant gap we need to fill to help control this pandemic.

Coronaviruses are a large family of single-stranded enveloped RNA viruses, which can be divided into four major genera, including Alphacoronavirus, Betacoronavirus, Gammacoronavirus, and Deltacoronavirus.[2] SARS-CoV and SARS-CoV-2 belong to the β-genus. Cutting-edge science allowed the rapid isolation of the SARS-CoV-2 and the sequencing of its viral genome.[3] The spike (S) glycoprotein trimer has been identified as a critical target to neutralize the virus and is the leading viral antigen used in many vaccines.[4] The virus uses the S glycoprotein to first attach to its functional receptor, human angiotensin-converting enzyme 2 (hACE2),[5−7] and then enters the host cell through the endocytic pathway.[8] hACE2 is broadly expressed on the surface of epithelial cells lining the upper and lower respiratory tract.[5] The interaction between SARS-CoV-2 S glycoprotein receptor-binding domain (RBD) and hACE2 regulates both the cross-species and human-to-human transmissions of SARS-CoV and SARS-CoV-2.

In the last 10 years, several structures of SARS-CoV S glycoprotein RBD in complex with hACE2 have been solved, for example, Protein Data Bank (PDB): 2AJF.[7,9−11] Additionally, the structure of SARS-CoV-2 trimeric S glycoprotein in complex with receptor hACE2 (PDB: 7DF4) (Figure 1A,B) has been recently reported.[12] These structures have revealed that SARS-CoV RBD and SARS-CoV-2 RBD enclose a core structure and a receptor-binding motif (RBM), which binds to the outer surface of the claw-like structure of hACE2 (Figure 1B).[10] It has also been reported that hACE2 binds to SARS-

Received: February 10, 2022
Accepted: July 6, 2022
Published: August 9, 2022

https://doi.org/10.1021/acsomega.2c00844
ACS Omega 2022, 7, 28779−28789

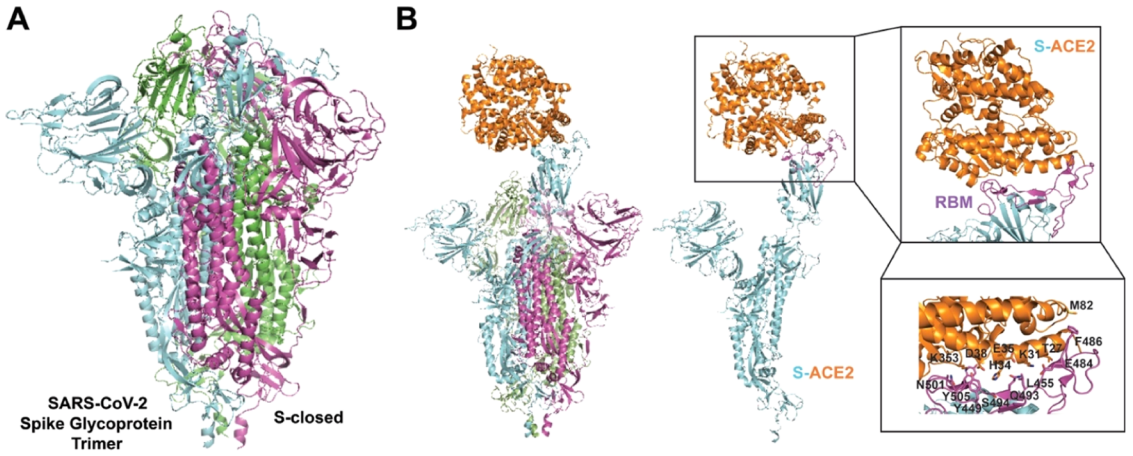

Figure 1. SARS-CoV-2 Recognizes Human ACE2. (A) Closed conformation of SARS-CoV-2 S glycoprotein trimer, S-closed (PDB: 7DF4). The three protomers 1, 2, and 3 are shown in cyan, magenta, and green, respectively; (B) Left: Overall structure of human SARS-CoV-2 S glycoprotein RBD in complex with hACE2, showing that the RBD of protomer 1 rotates 73.2° to 68.6° upward and outward during the open and binding states, respectively.[12] Only protomer 1 is up and binds to one hACE2, while the other two RBD protomers remain downward. Right: Overall view of protomer 1 (cyan) bound to hACE2 from SARS-CoV-2 S glycoprotein RBD-hACE2 complex. Close-up view of the three-dimensional (3D) structure of the interface between SARS-CoV-2 RBD and hACE2, in including main interactions. Figures were made using PyMOL.[46]

CoV-2 RBD (Pro330-Pro521) and SARS-CoV RBD with K_D of 1.2 and 5.0 nM, respectively.[13−18] These high-affinity bindings make the S glycoprotein mediate viral entry into human cells with high efficiency.[11] Fourteen key positions for binding SARS-CoV RBD to hACE2 are T402, R426, Y436, Y440, Y442, L472, N473 Y475, N479, Y484, T486, T487, G488, and Y491.[10] Eight of these positions are strictly conserved in SARS-CoV-2 RBD, whereas the other six positions are (semi)conserved: $R426_{\text{SARS-CoV}}N439_{\text{SARS-CoV-2}}$, $Y442_{\text{SARS-CoV}}L455_{\text{SARS-CoV-2}}$, $L472_{\text{SARS-CoV}}F486_{\text{SARS-CoV-2}}$, $N479_{\text{SARS-CoV}}Q493_{\text{SARS-CoV-2}}$, $Y484_{\text{SARS-CoV}}Q498_{\text{SARS-CoV-2}}$, and $T487_{\text{SARS-CoV}}N501_{\text{SARS-CoV-2}}$.[13] The conservation of many key contact residues could explain the similar binding affinities of SARS-CoV-2 RBD and SARS-CoV RBD for hACE2. Furthermore, based on the structural analysis by Wan et al.,[19] Gln493 in SARS-CoV-2 S glycoprotein was predicted to bind to the hACE2 virus-binding hot spot Lys31, which forms an intramolecular salt bridge with Glu35 buried in a hydrophobic environment. In addition, Asn501 of SARS-CoV-2 was predicted to bind to the hACE2 virus-binding hot spot Lys353 that engages in an intramolecular salt bridge with Asp38 also buried in a hydrophobic environment. Altogether, these results indicate that SARS-CoV-2 could adapt to the hACE2 ortholog 2002−2003 epidemic strains as SARS-CoV does, explaining the effective fusion mediated by their respective S glycoproteins and transmissibility in humans.[13]

To the best of our knowledge, few drugs have been described to have selective anti-SARS-CoV-2 activity, including remdesevir (EC_{50} = 0.77 μM; CC_{50} > 100 μM; therapeutic index (TI) > 129.87), which was initially designed to treat Ebola virus,[20−22] Oseltamivir, commonly used to treat influenza viruses;[23] arbidol and lopinavir/ritonavir,[24] darunavir and hydroxychloroquine,[25] favipiravir (EC_{50} = 61.88 μM, CC_{50} > 400 μM, TI > 6.46),[26] ribavirin (EC_{50} = 109.50 μM, CC_{50} > 400 μM, TI > 3.65),[27,28] nitazoxanide (derivative of tizoxanide, EC_{50} = 2.12 μM, CC_{50} > 35.53 μM, TI > 16.76),[29,30] and chloroquine (EC_{50} = 1.13 μM, CC_{50} > 100 μM, TI > 88.50).[22,31] In a computational study, binding between various functional proteins of SARS-CoV-2 with saquinavir, remdesivir, dolutegravir, and bictegravir has been investigated.[32] Another simulation study predicted derivatives of drugs tizoxanide, dolutegravir, bictegravir, and arbidol (Ti-2, BD-2, and Ar-3) as potential antivirals to target the SARS-CoV-2 S glycoprotein.[33] Other small molecules have also been identified as effective entry inhibitors of SARS-CoV-2 through drug repurposing screening and virtual screening (e.g., ingenol and cepharanthine).[34,35] In addition, small-molecule entry blockers targeting the fusion peptide[36] (chlorcyclizine, clobenztropine, D3-βArr) and the RBD[37−39] (MU-UNMC-1: IC_{50} = 0.67 μM, MU-UNMC-2: IC_{50} = 1.72 μM; H69C2: IC_{50} = 85.75 μM; DC-RA016: IC_{50} = 22.44 μM, DC-RA052: IC_{50} = 68.00 μM) of SARS-CoV-2 S glycoprotein have been identified. More recently, Merck and Pfizer obtained emergency approvals for Molnupiravir[40] and Paxlovid[41] COVID-19 antiviral pills, but none of them interfere with the SARS-CoV-2 S glycoprotein binding to the receptor. Although there has been progress in discovering anti-SARS-CoV-2 drugs, there is no ideal antiviral drug for prophylaxis or treatment of COVID-19 and/or prevention of transmission SARS-CoV-2. Small organic molecules are among the compounds that could be tested for potential selective antiviral activity. Their potential to disrupt the interaction between SARS-CoV-2 S glycoprotein RBD and hACE2 is of keen interest. We hypothesize that small molecules could disrupt the interaction of S glycoprotein with hACE2 and inhibit viral entry. Thus, we first analyzed the SARS-CoV-2 S glycoprotein RBD-hACE2 complex structure (PDB: 7DF4) and created models for different viral variants using visual molecular dynamics (VMD)[42] and molecular operating environment (MOE).[43] We then conducted a hit search using structure-based molecular docking virtual screening of commercially available small molecules (eMolecules database)[44] against the SARS-CoV-2 S glycoprotein RBD models using OEDocking FRED-4.0.0.0 software.[45] The best candidate compounds were purchased and tested using a SARS-CoV-2 pseudotyped cell-based assay. Three of these compounds, alone or in combination, showed antiviral selectivity.

https://doi.org/10.1021/acsomega.2c00844
ACS Omega 2022, 7, 28779−28789

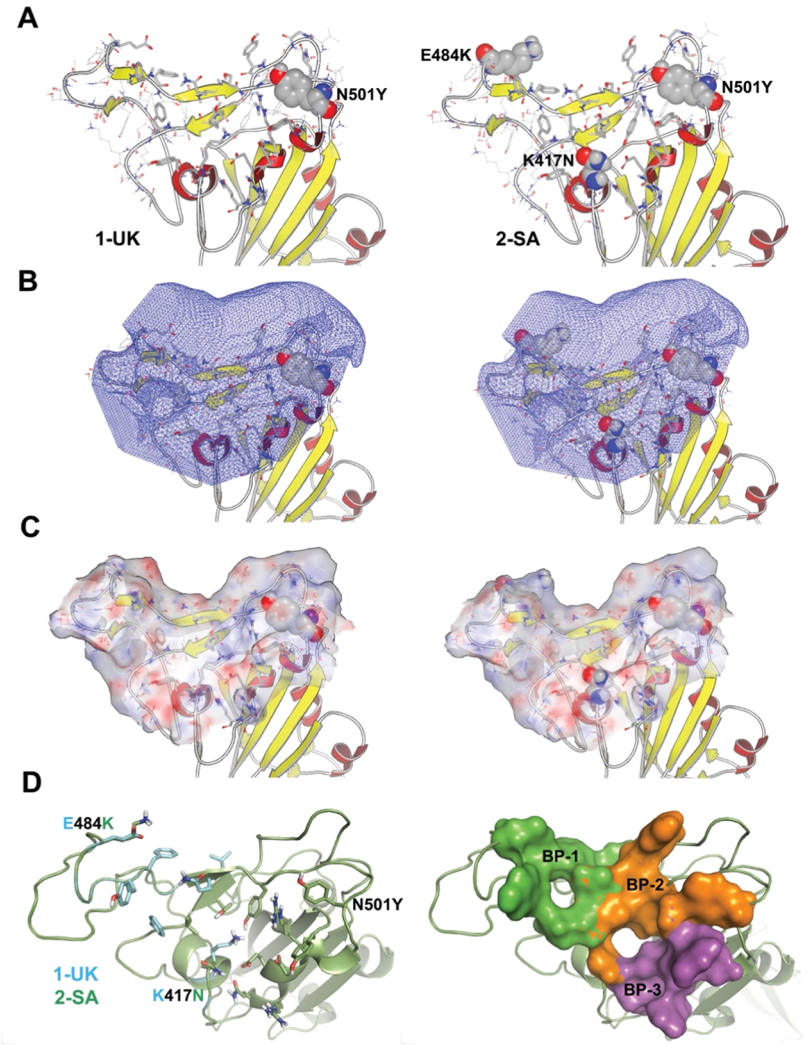

Figure 2. SARS-CoV-2 S Glycoprotein Models and Grid Boxes to Conduct Molecular Docking. (A) Model 1—α (United Kingdom, 1-UK) → N501Y | B.1.1.7, and Model 2—β (South Africa, 2-SA) → K417N, E484K, N501Y | B.1.351; (B) grid boxes built on each model to conduct molecular docking; (C) models 1-UK and 2-SA RBD molecular surfaces; (D) three binding pockets (BP-1, BP-2, and BP-3) were identified as a result of the molecular docking runs. Figures were made using OpenEye VIDA[45] and PyMOL.[46]

2. RESULTS

2.1. Computational and Experimental Studies. *2.1.1. SARS-CoV-2 S Glycoprotein RBD Models.* Figure 2A shows the two SARS-CoV-2 S glycoprotein RBD models created [α (United Kingdom, UK)@N501Y | B.1.1.7 (Model 1-UK); β (South Africa, SA)@K417N, E484K, N501Y | B.1.351 (Model 2-SA)] and used to conduct the structure-based molecular docking virtual screening (see the Supporting Information). The two models, 1-UK and 2-SA, have the N501Y mutation but differ in K417N and E484K mutations. Using these two models helped us in the search to discover various potential binders, increasing the likelihood of finding broad-spectrum antivirals and/or small-molecule probes to investigate the biology of SARS-CoV-2 further.

2.1.2. Molecular Docking and Experimental Studies. Two grid boxes were built for each model, 1-UK and 2-SA, to conduct the molecular docking studies, shown in Figure 2B. The selection was big enough to enclose the SARS-CoV-2 S glycoprotein RBD-hACE2 protein−protein interaction (PPI) molecular surface. The molecular docking run analysis shed insight into the number of binding pockets each model could allocate for potential binders to SARS-CoV-2 S glycoprotein RBD. The molecular surfaces for each of the SARS-CoV-2 S glycoprotein RBD models, 1-UK and 2-SA, are also shown in Figure 2C. Overall, mainly three common binding pockets between the two models, 1-UK and 2-SA, were identified as shown in Figure 2D. The residues surrounding the environment of each binding pocket are listed in Table 1.

The FRED-4.0.0.0 Chemguass4 scoring function[45] was then used to rank the screened molecules based on their affinities toward the SARS-CoV-2 S glycoprotein RBD. For models 1-UK and 2-SA, the Chemguass4 scoring function for the 10,000 top-ranked small molecules varies between −9.53 and −6.29

Table 1. Identified Binding Pockets | SARS-CoV-2 S Glycoprotein RBD-hACE2 PPI Molecular Surface

binding pocket	residues
1	Leu452|Leu455|Phe456|Glu484Lys|Tyr489|Phe490|Gln493
2	Arg403|Lys417Asn|Tyr449|Tyr453|Leu455|Gln493|Ser494|Tyr495|Asn501Tyr
3	Arg403|Asp405|Glu406|Arg408|Gln409|Lys417Asn|Gly504|Tyr505

https://doi.org/10.1021/acsomega.2c00844
ACS Omega 2022, 7, 28779−28789

Table 2. Ten (Out of 32 Compounds) Top-Ranked Binder Compounds toward SARS-CoV-2 S Glycoprotein RBD Mutant's Models

compound[a]	eMolecules ID[44]	molecular weight (g/mol)	Chemguass4 scoring function (kcal/mol)	SARS-CoV-2 S glycoprotein RBD mutant's models[b]	binding pocket[c]
HCC1	1540649	341.47	−8.3018 (>−6.2905|−3.3176)[d]	2-SA	3
HCC2	46070913	260.34	−7.9655 (>−6.2905)[d]	2-SA	2−3
HCC3	177461967	287.34	−9.5871 (−7.9199)	2-SA	2
HCC4	43606039	335.45	−8.7715 (>−6.2905|−5.2966)[d]	2-SA	2
HCC6	177360934	274.33	−8.9569 (−9.4625)	2-SA	2
HCC7	68885577	342.40	−7.2996 (>−7.5860)[e]	1-UK	2
HCC8	46033143	254.35	−7.8840 (>−6.2905)[d]	2-SA	2−3
HCC11	49646512	337.38	−7.2378 (>−7.5860|−6.5239)[e]	1-UK	1 (2−3)[f]
HCC14	177358552	303.37	−7.9444 (−7.7349)	1-UK	2
HCC19	49044086	300.36	−8.3116 (>−6.2905)[d]	2-SA	2

[a]The tested compounds were purchased from Chemspace LLC. https://chem-space.com and/or ChemBridge | Hit2Lead. https://www.hit2lead.com. [b]The specific model, 1-UK or 2-SA, where the compounds were initially identified within the 10,000 top-ranked molecules from each docking run. [c]The binding pocket occupied in the model, 1-UK or 2-SA, where the compounds were initially identified. [d]These compounds were not selected within the 10,000 top-ranked ones for model 1-UK, where the Chemgauss4 scoring function's lower value is −6.2905 kcal/mol. [e]These compounds were not selected within the 10,000 top-ranked ones for model 2-SA, where the Chemgauss4 scoring function's lower value is −7.5860 kcal/mol. For HCC1 and HCC4, and HCC11 molecular dockings were re-performed against models where they were not identified initially, that is, 1-UK, and 2-SA, respectively. Overall, the FRED-4.0.0.0 Chemguass4 scoring function is lower for model 2-SA compared to model 1-UK. [f]In model 2-SA, HCC1 binds within binding pocket BP-3 and portion of BP-2.

Table 3. Biological Activity of the Three Top-Ranked Binder Compounds toward SARS-CoV-2 S Glycoprotein RBD Mutants

	CC_{50}[b]	EC_{50}[c]			
compound[a]	μM (95% confidence interval)		TI[d] (CC_{50}/EC_{50})	Chemguass4 scoring function (kcal/mol)	SARS-CoV-2 S glycoprotein RBD model[e]
HCC1	391.5 (207.9−873.2)	125.6 (57.0−330.3)	3.1	−8.3018	2-SA
HCC4[f]	515.7 (258.1−1365.9)	128.2 (74.4−236.9)	4.0	−8.7715	2-SA
HCC11	>74.1	26.7 (11.9−77.4)	>8.2	−7.2378	1-UK
HCC1+4	184.3 (101.1−361.1)	13.5 (8.8−20.5)	13.7	N/A[g]	2-SA
HCC1+11	227.2 (112.6−522.4)	30.4 (14.2−64.6)	7.5	N/A	1-UK|2-SA
HCC4+11	627 (264.2−2966.5)	58.9 (32.7−109.9)	10.6	N/A	1-UK|2-SA
HCC1+4+11	121.5 (52.9−135.1)	13.3 (8.8−20.1)	9.1	N/A	1-UK|2-SA
i-carrageenan[h]	>362.5	1.899 (1.261−2.854)	>190	N/A	N/A

[a]The tested compounds were purchased from Chemspace LLC. https://chem-space.com and/or ChemBridge | Hit2Lead. https://www.hit2lead.com. [b]CC_{50}: half-maximal cytotoxic concentration. [c]EC_{50}: half-maximal effective concentration. [d]TI: therapeutic index. [e]The specific RBD model, 1-UK or 2-SA, where the compounds were initially identified within the 10,000 top-ranked molecules from each docking run. [f]Racemic mixture. [g]N/A: not available. [h]Average molecular weight of *i*-carrageenan is 551.80 g/mol.

kcal/mol and −10.87 and −7.59 kcal/mol, respectively. Overall, the FRED-4.0.0.0 Chemguass4 scoring function is lower for model 2-SA compared to model 1-UK. The best ∼50 candidate compounds, including both models, 1-UK and 2-SA, were prioritized to be tested experimentally. Thirty-two of these compounds were commercially available, purchased, and later experimentally tested using the SARS-CoV-2 spike pseudotyped lentivirus assay.

2.1.3. Cytotoxicity and Antiviral Assay. Table 2 lists the 10 top-ranked compounds including both models, 1-UK and 2-SA, that showed some promising antiviral activity in a preliminary screening binding assay together with their predicted FRED-4.0.0.0 Chemgauss4 scoring function. These top-ranked compounds were tested in the pseudoviral model, and only the three top-ranked binder compounds (HCC1, HCC4, and HCC11) that have been predicted to bind to three different binding pockets (BP-1, BP-2, and BP-3) and showed potential EC_{50s} under 200 μM in the preliminary pseudoviral assay were selected for further analysis, HCC1, HCC4, and HCC11. The half-maximal cytotoxic concentration (CC_{50}), half-maximal effective concentration (EC_{50}), and therapeutic index (TI) were determined using the XTT colorimetric assay, SARS-CoV-2 pseudotyped cell-based assay, and the CC_{50}/EC_{50} ratio, respectively (Table 3). *i*-carrageenan was used as positive control (Table 3). HCC11 shows the best activity in the SARS-CoV-2 pseudoviral model with an EC_{50} of 26.7 μM. HCC1 and HCC4 follow with EC_{50} of 125.6 μM and 128.2 μM, respectively. These compounds alone show low therapeutic indices (TI), ranging between 3.1 and >8.2 (see Table 3). However, when the compounds were combined, their EC_{50} and TI values were improved. For example, combining HCC1 and HCC4 resulted in lower EC_{50} and higher TI values (over 9-fold lower for the EC_{50} value and 4-fold higher for the TI value). Similarly, the combination of HCC1 and HCC11 or HCC1, HCC4, and HCC11 produced lower EC_{50} values.

2.2. Molecular Interactions and Optimization. *2.2.1. SARS-CoV-2 S Glycoprotein RBD-HCC11 Complex Model.* The predicted SARS-CoV-2 S glycoprotein RBD-HCC11 complex model was obtained through molecular docking studies using both models, 1-UK and 2-SA. In model 1-UK, the main interactions between SARS-CoV-2 S

https://doi.org/10.1021/acsomega.2c00844
ACS Omega 2022, 7, 28779−28789

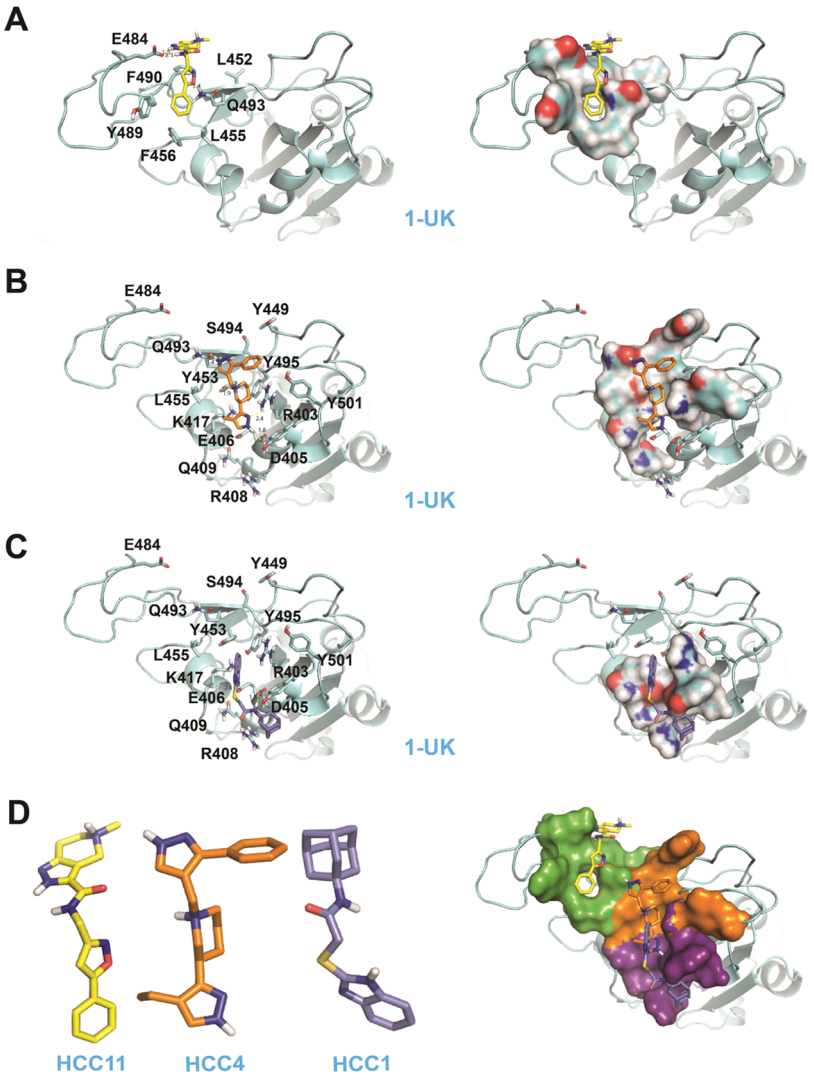

Figure 3. SARS-CoV-2 S glycoprotein−compound complex models using mutant model 1-UK. (A) SARS-CoV-2 S glycoprotein RBD-HCC11 complex model; (B) SARS-CoV-2 S glycoprotein RBD-HCC4 complex model; (C) SARS-CoV-2 S glycoprotein RBD-HCC1 complex model. SARS-CoV-2 S glycoprotein RBD−compound main interactions through hydrogen bonds are shown as yellow dashed lines. (D) Left: 3D structure of identified compounds: HCC11, HCC4, and HCC1. Right: predicted binding poses of compounds HCC11, HCC4, and HCC1 on their binding pockets (BP-1, green; BP-2, orange; and BP-3, purple). Figures were made using PyMOL.[46]

glycoprotein RBD-HCC11(5-methyl-*N*-[(5-phenylisoxazol-3-yl)methyl]-4,5,6, 7-tetrahydro-1*H*-pyrazolo[4,3-*c*]pyridine-3-carboxamide) complex are depicted in Figure 3A. HCC11 binds within binding pocket BP-1 (see Table 2) and engages in three hydrogen bonds (HBonds) with the side-chain carboxylate group of Glu484 (2 HBonds) and the side-chain amine group of Gln493 of SARS-CoV-2 S glycoprotein RBD via its hydrogen-donor pyrrole-like nitrogen group, peptide chain nitrogen (amide group), and 1,2 oxasole ring, respectively. HCC11's benzene group engages in hydrophobic and aromatic interactions with Leu455, Phe456, and Tyr489. HCC11's pyrazole and piperidine rings engage in hydrophobic and aromatic interactions with Phe490. Some of these residues, including Leu455, Phe456, Gln493, and Tyr489, have also been identified as hotspot residues in recent molecular dynamics studies,[47−49] which support our computational predictions. It is worth highlighting that Lys417 and Glu484 present in the α variant of SARS-CoV-2 (model 1-UK) are mutated to Asn417 and Lys484, respectively, in the β variant SARS-CoV-2 (model 2-SA). Thus, in model 2-SA, HCC11 is predicted to bind within binding pocket BP-3 and portion of BP-2 (see Table 2 and Figure 4A,D, right). The main interactions between SARS-CoV-2 S glycoprotein RBD-HCC11complex are depicted in Figure 4A. HCC11 engages in four hydrogen bonds with the side-chain carboxylate group of Glu406 (2 HBonds), the side-chain hydroxyl group of Tyr453, and the side-chain hydroxyl group of Tyr505 of SARS-CoV-2 S glycoprotein RBD via its peptide chain nitrogen (amide group) and hydrogen-donor pyrrole-like nitrogen group, piperidine ring, and 1,2 oxasole ring, respectively. HCC11's benzene group engages in hydrophobic interactions with Arg408. HCC11's peptide chain nitrogen (amide group), pyrazole and piperidine rings engage in hydrophobic and aromatic interactions with Arg403, Asn417, Tyr453, and Tyr495. It is worth pointing out that the above key residues identified in SARS-CoV-2 S glycoprotein RBD-HCC11 recognition coincide with hotspot resides described previously such as Lys417Asn, Tyr495, and Tyr505.[47,48] The HCC11's Chemgauss4 scoring functions against model 1-UK (BP-1) and model 2-SA (BP-3 and portion of BP-2) are comparable, −7.24

https://doi.org/10.1021/acsomega.2c00844
ACS Omega 2022, 7, 28779−28789

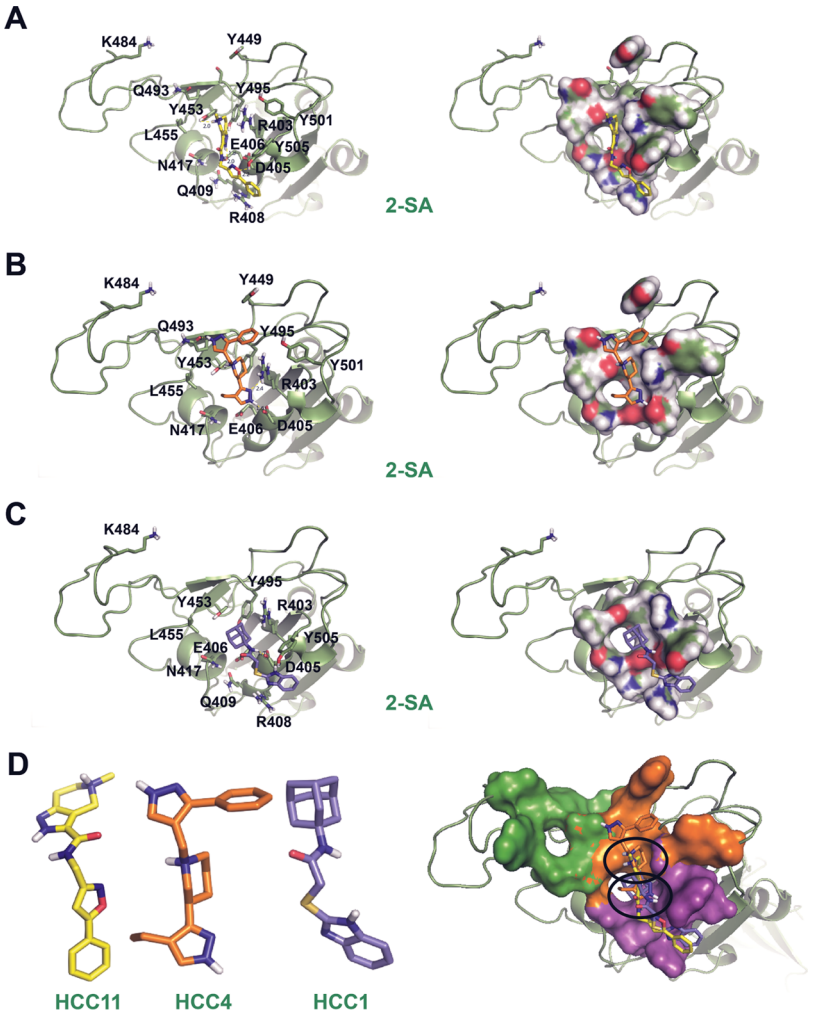

Figure 4. SARS-CoV-2 S Glycoprotein−compound complex models using mutant model 2-SA. (A) SARS-CoV-2 S glycoprotein RBD-HCC11 complex model; (B) SARS-CoV-2 S glycoprotein RBD-HCC4 complex model; (C) SARS-CoV-2 S glycoprotein RBD-HCC1 complex model. SARS-CoV-2 S glycoprotein RBD-compounds main interactions through hydrogen bonds are shown as yellow dashed lines. (D) Left: 3D structure of identified compounds: HCC11, HCC4, and HCC1. Right: predicted binding poses of compounds HCC11, HCC4, and HCC1 on their binding pockets (BP-2, orange; and BP-3, purple). The HCC4's pyrazole and HCC1's adamantane (tricyclo dodecane) groups overlap in a shared subpocket located on the border between BP-2 and BP-3 as depicted with the lower black ellipse. They both interact with Asp405 through hydrogen bond. Likewise, the predicted binding poses of HCC4 and HCC11 also revealed a partial overlap between both compounds as depicted with the upper black ellipse. See Section 2.2 for further explanation. Figures were made using PyMOL.[4]

and −6.52 kcal/mol, respectively (see Table 2). However, as mentioned above, for the 10,000 top-ranked molecules, the Chemguass4 scoring function is lower for model 2-SA compared to model 1-UK. Altogether, HCC11 might bind within different binding pockets in model 1-UK and model 2-SA due to the Lys417Asn and Glu484Lys mutations.

2.2.2. SARS-CoV-2 S Glycoprotein RBD-HCC4 Complex Model. The predicted SARS-CoV-2 S glycoprotein RBD-HCC4 complex model was obtained through molecular docking studies using both models, 1-UK and 2-SA. The main interactions between SARS-CoV-2 S glycoprotein RBD-HCC4 (3-(4-ethyl-1*H*-pyrazol-5-yl)-1-[(3-phenyl-1*H*-pyrazol-4-yl)methyl]piperidine) complex are depicted in Figures 3B and 4B. In both models, 1-UK and 2-SA, HCC4 binds within binding pocket BP-2 (see Table 2) and engages in four hydrogen bonds with the side-chain guanidino group of Arg403, the side-chain carboxylate group of Asp405, the side-chain hydroxyl group of Tyr453, and the side-chain carbonyl group of Gln493 of SARS-CoV-2 S glycoprotein RBD via its pyrazole ring (2 HBonds), central piperidine ring, and another pyrazole ring, respectively. HCC4's central piperidine ring engages in hydrophobic interactions with Arg403, Tyr453, and Tyr495. HCC4's benzene group engages in hydrophobic and aromatic interaction with Arg403, Tyr449, and Tyr501. The HCC4's ethyl group in the pyrazole ring engages in hydrophobic interactions with Lys417 (Model 1-UK) or Asn417 (Model 2-SA). The ethyl pyrazole ring is also surrounded by Arg403 and Tyr505. It is important to mention that HCC4's Chemgauss4 scoring function in model 1-UK (−5.30 kcal/mol; Lys417) is much higher compared to model 2-SA (−8.77 kcal/mol; Asn417) likely caused by the Lys417Asn mutation and steric hindrance by Lys417 in the binding vicinity in model 1-UK (see Table 2 and Figures 3B and 4B). Some residues predicted for the recognition of HCC4 by SARS-CoV-2 S glycoprotein RBD have also been recently described via molecular dynamics simulation studies as hotspots including Lys417Asn, Tyr449, Gln493, Tyr495, Tyr501, and Tyr505.[47,48] It is also worth remarking that

https://doi.org/10.1021/acsomega.2c00844
ACS Omega 2022, 7, 28779−28789

Tyr501 is the result of mutation Asn501Tyr that is exhibited for SARS-CoV-2 α and β variants and is included in our both SARS-CoV-2 S glycoprotein RBD models, 1-UK and 2-SA.

2.2.3. SARS-CoV-2 S Glycoprotein RBD-HCC1 Complex Model. The predicted SARS-CoV-2 S glycoprotein RBD-HCC1 complex model was obtained through molecular docking studies using both models, 1-UK and 2-SA. In model 1-UK, the main interactions between SARS-CoV-2 S glycoprotein RBD-HCC1 (*N*-1-adamantyl-2-(1*H*-benzimidazol-2-ylthio)acetamide) complex are depicted in Figure 3C. HCC1 binds within binding pocket BP-3 and engages in two hydrogen bonds with the side-chain carboxylate group of Asp405 and the side-chain carboxylate group of Glu406 of SARS-CoV-2 S glycoprotein RBD via its peptide chain nitrogen (amide group) and the imidazole ring, respectively. The adamantane (tricyclo dodecane) group at one end of the HCC1 is sandwiched through hydrophobic interactions between residues Arg408 and Tyr505. In model 2-SA, HCC1 is flipped compared to the binding pose obtained in model 1-UK. The main interactions between SARS-CoV-2 S glycoprotein RBD-HCC1 (*N*-1-adamantyl-2-(1*H*-benzimidazol-2-ylthio)acetamide) complex are depicted in Figure 4C. HCC1 binds within binding pocket BP-3 (see Table 2) and engages in two hydrogen bonds with the side-chain carboxylate group of Asp405 and the side-chain hydroxyl group of Tyr505 of SARS-CoV-2 S glycoprotein RBD via its peptide chain nitrogen (amide group) and the imidazole ring, respectively. The adamantane (tricyclo dodecane) group at one end of the HCC1 sits in a pocket surrounded by a network of hydrophobic interactions including residues Leu455, Tyr453, Tyr495, Asn417, Glu406, and Arg403. It is worth mentioning that Tyr505 plays a key role in the binding of hACE2 to SARS-CoV-2 S glycoprotein RBD. A single-mutation Tyr505Ala is sufficient to abolish the binding between SARS-CoV-2 S glycoprotein RBD and hACE2.[12] Besides Tyr505, other residues identified here as key for the SARS-CoV-2 S glycoprotein RBD-HCC1 interaction coincide with those described recently as hotspots using molecular dynamics simulations, which are Lys417Asn, Leu455, Tyr495.[47,48] The HCC1's Chemgauss4 scoring functions against model 1-UK (BP-3) and model 2-SA (BP-3) are different, −3.32 and −8.30 kcal/mol, respectively (see Table 2). This is likely to be caused by the Lys417Asn mutation, where the HCC1's adamantane group might not fit well in the vicinity of Lys417 in model 1-UK, but does within the vicinity of Asn417.

In model 2-SA, the predicted binding poses of HCC1 and HCC4 in complex with SARS-CoV-2 S glycoprotein RBD revealed a partial overlap between both compounds (see Figure 4D, right). Specifically, the HCC4's pyrazole and HCC1's adamantane (tricyclo dodecane) groups overlay in a shared subpocket located on the border between binding pocket BP-2 and binding pocket BP-3. As mentioned above, these two groups interact with the side-chain carboxylate group of Asp405 through respective hydrogen bonds. This finding could provide a good starting point for a successful computer-aided molecular design and chemical optimization of HCC1−4. For instance, the HCC4's pyrazole and HCC1's adamantane (tricyclo dodecane) groups could be bred while keeping the amine group from either the pyrazole ring (HCC4) or the chain peptide amine (HCC1). A library of compounds made with different substituents (i.e., hydrophobic, aromatics, and/or electrostatics-mediated interaction groups) in the vicinity of the HCC1−4 bred portion is being designed and studied computationally to be synthesized and tested experimentally. Likewise, in model 2-SA, the predicted binding poses of HCC4 and HCC11 in complex with SARS-CoV-2 S glycoprotein RBD also revealed a partial overlap between both compounds (see Figure 4D, right). Chemical optimization of HCC4−11 could take place by breeding the HCC4's (3-phenyl-1*H*-pyrazol-4-yl)methyl and the HCC11's piperidine groups. This structure-based rational design also takes advantage of the subpocket between the two binding pockets BP-2 and BP-3 to be better occupied. Overall, the identification of all of these compounds and their combination could open the door for further structure-based rational design and optimization, including new analogues search, to achieve enhanced affinity, selectivity, and low cytotoxicity.

DISCUSSION

This study used an interdisciplinary approach combining computational biophysics, structure-guided design, and experimental virological bioassays to discover neutralizing agents targeting the SARS-CoV-2 S glycoprotein RBD. The SARS-CoV-2 pseudoviral model is widely used to test the antiviral activity of compounds that interfere with viral attachment or entry to target cells. Our assay used iota carrageenan as a positive control for a compound that interferes with SARS-CoV-2 entry to target cells. Carrageenan is currently being evaluated in a clinical trial as a potential treatment to prevent COVID-19 illness.[50] Carrageenan is a sulfated polysaccharide that may bind to positively charged patches on the viral spike producing a shielding effect on viral attachment and entry.[51] The overall approach used in this study (i.e., screen million molecules, select top-ranked molecules, and test them experimentally) is comparable to other recent successful studies aimed at discovering SARS-CoV-2 S glycoprotein RBD inhibitors.[38,52,53] Specifically, here, we screened a commercially available small molecules database (i.e., an in-house prepared set of eMolecules lead-like database of ∼4.3 million compounds[44]) against two SARS-CoV-2 S glycoprotein RBD models, 1-UK and 2SA, using structure-based molecular docking high-throughput virtual screening. About 30% of the compounds tested experimentally (10 out of 32) showed affinity toward SARS-CoV-2 S glycoprotein RBD. Three of these compounds, alone or in combination, displayed antiviral selectivity with EC_{50s} in the mid-low micromolar concentration, although with low therapeutic indices (see Table 3). These compounds bind to different binding pockets within the large binding site enclosing the SARS-CoV-2 S glycoprotein RBD-hACE2 PPI molecular surface. One compound, HCC1, interacts via hydrogen bond with Tyr505, a key residue recognizing hACE2.[12] The other compound, HCC11, is predicted to engage with Glu484 via a hydrogen bond in the α variant (Model 1-UK), mutated to Lys484 in the SARS-CoV-2 β variant. In this latter variant, model 2-SA, HCC11 is predicted to bind to Tyr505, which plays a key role in the binding of hACE2 to SARS-CoV-2 S glycoprotein RBD. A single-mutation Tyr505Ala is sufficient to abolish the binding between SARS-CoV-2 S glycoprotein RBD and hACE2.[12]

Schmidt and collaborators identified potential naturally occurring mutations in the spike protein using HIV-1 pseudotypes and plasma selection experiments with vesicular stomatitis virus/SARS-CoV-2 chimeras.[54] This experiment identified several mutations that may occur naturally in the RBD section of the spike protein. These mutations include K378R, K444T, V445E/M, G446R, N450D, E484K, and

https://doi.org/10.1021/acsomega.2c00844
ACS Omega 2022, 7, 28779−28789

Q493R. The Q493 is the only amino acid listed in Table 1 and is involved in binding pocket BP-1. The analysis of these mutations using computational modeling (data not shown) concludes that they may not affect the binding of the lead molecules identified in this study, at least for the SARS-CoV-2 β variant (Model 2-SA); the one experimentally tested in this study.

Notably, the SARS-CoV-2 S glycoprotein RBD has been described as an immunodominant region due to the low level of glycosylation, compared to the rest of the S protein, and the higher accessibility on the surface of virions and virus-infected cells.[55] The regions analyzed in our study do not show potential sites of glycosylation that may interfere with the binding of the small molecule. Additionally, our pseudoviral model clearly shows that these molecules can inhibit pseudoviral entry in the low μM range.

These results are encouraging since discovering small molecules that can block the interaction between SARS-CoV-2 S glycoprotein RBD, and hACE2 is challenging due to the large PPI molecular surface. We identified common binding pockets between models 1-UK and 2-SA within the large PPI molecular surface utilized to perform structure-based molecular docking. Small molecules occupied at least three pockets in both models, 1-UK, and 2-SA. Since the combination of these small molecules shows a better antiviral activity (see Table 3), computer-aided drug design, fragment-based design, molecular breeding, and optimization approaches could be used to fuse these molecules and enhance their affinity and selectivity.

4. CONCLUSIONS

In summary, we conclude that the combined computational biophysics and experimental approach once again show to be reliable to discover high-affinity and selective small molecules against drug targets (i.e., SARS-CoV-2 S glycoprotein RBD). This study had an additional challenge, the large PPI molecular surface. However, we were able to identify three small molecules, HCC1,4,11, that alone or in combination provided a moderate antiviral activity against SARS-CoV-2 pseudovirus (PsV). This research also opens the doors to identifying highly potent and selective analogues and/or new derivatives. Overall, these small molecules may lead to effective antiviral treatments or serve as probes to better understand the biology of SARS-CoV-2. This research offers the foundation for future studies on the discovery and optimization of anti-SARS-CoV-2 small-molecule drugs.

5. EXPERIMENTAL SECTION

5.1. Computational Study. *5.1.1. Building the SARS-CoV-2 S Glycoprotein RBD Models.* Using the cryo-electron microscopy (cryo-EM) SARS-CoV-2 spike (S) glycoprotein receptor-binding domain (RBD)-hACE2 complex structure (Protein Data Bank (PDB): 7DF41), two SARS-CoV-2 S glycoprotein RBD models were built based on the main four different viral variants (Wuhan-USA-D614G, United Kingdom (UK)-B.1.1.7, Brazil-P.1, and South Africa-B.1.351) identified when this research began. The mutations for each of the variants were analyzed and incorporated in the models: Wuhan (United States)@D614G; α (United Kingdom, UK)@N501Y | B.1.1.7 (Model 1-UK); β (South Africa, SA)@K417N, E484K, N501Y | B.1.351 (Model 2-SA); γ (Brazil)@K417T, E484K, N501Y | P.1 using VMD.[42] MOE[43] was used to minimize and prepare each model by keeping all default parameters in the Protein Preparation module. Model 1-UK and model 2-SA were used to conduct structure-based virtual screening described in Section S1.2 (see Figure 2A).

5.1.2. Structure-Based High-Throughput Virtual Screening to Identify Small-Molecule Hit Compounds for SARS-CoV-2 S Glycoprotein RBD. We used structure-based molecular docking virtual screening to identify potential small-molecule hit compounds targeting SARS-CoV-2 S glycoprotein RBD. We screened an extensive and putatively unbiased commercially available database of small molecules (i.e., an in-house prepared set of eMolecules lead-like database of ~4.3 million compounds[44]) against two SARS-CoV-2 S glycoprotein RBD models (i.e., built based on PDB: 7DF4) using OEDocking FRED-4.0.0.0 software.[45] The docking studies were conducted with OEDocking FRED-4.0.0.0 software default parameters.[45] The grid was built encompassing all protein−protein interaction (PPI) molecular surfaces of the SARS-CoV-2 S glycoprotein RBD-hACE2 complex. The 10,000 highest-ranked molecules from each docking run were inspected, analyzed visually, and clustered. The top-ranked pose for each small molecule was selected for further analysis. The small molecules were ranked using the FRED-4.0.0.0 Chemguass4 scoring function based on their affinities. The OEDocking Report-4.0.0.0 was also used to guide the selection. Finally, over 50 highest-ranked molecules were prioritized to be tested experimentally using the SARS-CoV-2 spike pseudotyped assay (Section 2.2.2). The small molecules with the highest affinity would become the "hit/lead" compounds. The three-dimensional coordinates of SARS-CoV-2 S glycoprotein RBD-hACE2 complex structure (PDB: 7DF4) were downloaded from the Protein Data Bank database (https://www.rcsb.org, accessed on December 29, 2020).

5.2. Antiviral Activity. *5.2.1. Production and Purification of SARS-CoV-2 PsV.* SARS-CoV-2 pseudovirus (PsV) was produced as described by Schmidt et al.[56] Plasmids containing the SARS-CoV-2 spike gene [pSARS-CoV1-Strunc, pSARS-CoV2-Strunc (K417N/ E484K/N501Y mutations)], pCRV1NHG GagPol, and pNanoLuc2AEGFP were used to produce the pseudoviral particle and were kindly provided by Drs. Theodora Hatziioannou and Paul Bieniasz, Rockefeller University. The plasmids were used to transfect 293T cells (ATCC, Manassas, VA) monolayers prepared in six-well plates. Briefly, the DNA/lipofectamine 2000 (Thermo Fisher Scientific, Waltham, MA) mixtures were added to 293T cell monolayers and incubated for 6 h at 37 °C, 5% CO_2, and 98% humidity. The cell monolayers were then washed twice with D-PBS (Thermo Fisher Scientific) and finally incubated for 48 h at 37 °C, 5% CO_2, 98% humidity in Dulbecco's modified Eagle's medium (DMEM) (Thermo Fisher Scientific) with 10% FBS (Thermo Fisher Scientific) and Penicillin + Streptomycin (Thermo Fisher Scientific, Waltham, MA). After the 48 h incubation, the cell supernatants were collected, filtered (using a 0.22 μm pore size PVDF filter), aliquoted, and stored at −80 °C. The pseudoviral titer was determined using a cell-based pseudoviral entry assay[57] and the TurboLuc Luciferase One-Step Glow Assay Kit (Thermo Fisher Scientific).

5.2.2. Testing the New Molecules Targeting S Glycoprotein in a Cell-Based Antiviral Assay Using SARS-CoV-2 Pseudoviral Model. The human angiotensin-converting enzyme 2 (hACE-2)-expressing HeLa cells (HeLa ACE-2) were used to test the cytotoxicity and antiviral activity of the

https://doi.org/10.1021/acsomega.2c00844
ACS Omega 2022, 7, 28779−28789

compounds, alone or in combination. The cells were provided by Dr. Dennis Burton (The Scripps Research Institute, La Jolla, CA). The colorimetric XTT assay and the cell-based pseudoviral assays were performed to test cytotoxicity and antiviral activity, respectively, as previously described.[50] For the cytotoxicity assay, HeLa-ACE2 cells were exposed to different compound dilutions (alone or in combinations) or culture medium (DMEM with 10% fetal bovine serum and antibiotics) to serve as cell controls. After 72 h of incubation at 37 °C, 5% CO_2, and 98% humidity, cell viability was estimated using the XTT colorimetric assay. The 96-well microplates were read at 450 nm using the Spectramax iD3 microplate reader (Molecular Devices, San Jose, CA).

To test for antiviral activity, the different compound concentrations (alone or in combinations) tested in the cytotoxicity assay or cell culture medium (for virus control) were mixed with SARS-CoV-2 K417N/E484K/N501Y PsV. The mixture was transferred to 96-well white-opaque microplates (Thermo Fisher Scientific) containing HeLa-ACE2 cells. The plates were incubated for 72 h at 37 °C, 5% CO_2, and 98% humidity. The luciferase activity was tested using the TurboLuc One Step assay (Thermo Fisher Scientific), and luminescence was read in the Spectramax iD3 microplate reader. Iota carrageenan (Sigma-Aldrich, St. Louis, MO), a polysaccharide with potent activity against SARS-CoV-2, was included as a positive control in the SARS-CoV-2 pseudoviral model.

The raw data from the XTT and cell-based pseudoviral assays were analyzed using GraphPad Prism software version 9.0.2 (San Diego, CA; four-parameter dose−response curve) to obtain the CC_{50} and EC_{50} values. All extract dilutions and controls were tested in triplicate. CC_{50} and EC_{50} ratios were used to calculate the TI values. Compounds with TI values above 10 were considered potential candidates to further develop.

■ ASSOCIATED CONTENT

Supporting Information

The Supporting Information is available free of charge at https://pubs.acs.org/doi/10.1021/acsomega.2c00844.

Three top-ranked binder compounds toward SARS-CoV-2 S glycoprotein RBD UK mutant's model (Table S1); three top-ranked binder compounds toward SARS-CoV-2 S glycoprotein RBD SA mutant's model (Table S2); flexible alignment of three top-ranked binder compound structures (Table S3); comparison of predicted binding poses by OEDocking and MOE programs of SARS-CoV-2 S glycoprotein RBD−compound complex models using mutant model 1-UK (Figure S1); comparison of predicted binding poses by OEDocking and MOE programs of SARS-CoV-2 S glycoprotein RBD−compound complex models using mutant model 2-SA (Figure S2); flexible alignment and pharmacophore consensus of the top-ranked binder compounds, HCC11, HCC4, HCC1, structures (Figure S3); molecular dynamics simulation of SARS-CoV-2 S glycoprotein 1-UK RBD in complex with HCC11 (Figure S4); molecular dynamics simulation of SARS-CoV-2 S glycoprotein 2-SA RBD in complex with HCC11 (Figure S5); molecular dynamics simulation of SARS-CoV-2 S glycoprotein 2-SA RBD in complex with HCC4 (Figure S6); and molecular dynamics simulation of SARS-CoV-2 S glycoprotein 2-SA RBD in complex with HCC1 (Figure S7) (PDF)

■ AUTHOR INFORMATION

Corresponding Author

Yoel Rodríguez − *Department of Natural Sciences, Hostos Community College of The City University of New York, New York, New York 10451, United States; Department of Pharmacological Sciences, Icahn School of Medicine at Mount Sinai, New York, New York 10029, United States;* orcid.org/0000-0002-7334-7828; Email: yoel.rodriguez@mssm.edu

Authors

Scarlet Martínez Cardoze − *Department of Natural Sciences, Hostos Community College of The City University of New York, New York, New York 10451, United States*

Onyinyechi W. Obineche − *Department of Natural Sciences, Hostos Community College of The City University of New York, New York, New York 10451, United States*

Claudia Melo − *Department of Science, Borough of Manhattan Community College of The City University of New York, New York, New York 10007, United States; Brooklyn College of The City University of New York, New York, New York 11210, United States;* Present Address: George Washington University, Washington, District of Columbia 20052, United States; orcid.org/0000-0003-2663-1196

Ashanna Persaud − *Department of Science, Borough of Manhattan Community College of The City University of New York, New York, New York 10007, United States*

José A. Fernández Romero − *Department of Science, Borough of Manhattan Community College of The City University of New York, New York, New York 10007, United States; Center for Biomedical Research, The Population Council, New York, New York 10065, United States*

Complete contact information is available at: https://pubs.acs.org/10.1021/acsomega.2c00844

Author Contributions

The manuscript was written through contributions of all authors. All authors have given approval to the final version of the manuscript.

Funding

This research was funded by the CUNY Community College Research Grant (CCRG, No. 1738).

Notes

The authors declare no competing financial interest.

■ ACKNOWLEDGMENTS

S.M.C. and O.W.O. were supported by CCRG and the CUNY Research Scholars Program (CRSP), respectively, and thank the National Science Foundation (NSF S-STEM Award DUE-1833767). The authors are grateful to Dr. Theodora Hatziioannou and Dr. Paul Bieniasz of The Rockefeller University who kindly provided the plasmids to produce SARS-CoV-2 PsV. C.M. was funded by the National Institutes of Health Maximizing Access to Research Careers Program (award #5T34GM008078-31). Y.R. thanks Dr. Mercedes Martín-Martínez (Instituto de Química Médica [IQM], Spanish National Research Council [CSIC]—Madrid, Spain) for helpful discussions, and is grateful to PSC CUNY grant

https://doi.org/10.1021/acsomega.2c00844
ACS Omega 2022, 7, 28779−28789

(award #TRADB-50-500). The authors are thankful to OpenEye Scientific Software for providing free academic license. Computations were supported in part through the computational resources and staff expertise provided by the Scientific Computing Facility at the Icahn School of Medicine at Mount Sinai.

■ ABBREVIATIONS

SARS-CoV-2, severe acute respiratory syndrome coronavirus 2; COVID-19, coronavirus diseases 2019; HCC, Hostos Community College; RBD, receptor-binding domain; hACE2, human angiotensin-converting enzyme 2; RBM, receptor-binding motif; PDB, Protein Data Bank; PPI, protein−protein interaction; HBond, hydrogen bonds; CC_{50}, half-maximal cytotoxic concentration; EC_{50}, half-maximal effective concentration; IC_{50}, half-maximal inhibitory concentration; TI, therapeutic index

■ REFERENCES

(1) WHO. Coronavirus Disease 2019 (COVID-19) Situation Report—Weekly epidemiological Update on COVID-19, 2021. https://www.who.int/emergencies/diseases/novel-coronavirus-2019/situation-reports.
(2) Perlman, S.; Netland, J. Coronaviruses post-SARS: update on replication and pathogenesis. *Nat. Rev. Microbiol.* **2009**, *7*, 439−450.
(3) Zhu, N.; Zhang, D.; Wang, W.; Li, X.; Yang, B.; Song, J.; Zhao, X.; Huang, B.; Shi, W.; Lu, R.; et al. A Novel Coronavirus from Patients with Pneumonia in China, 2019. *N. Engl. J. Med.* **2020**, *382*, 727−733.
(4) Hoffmann, M.; Kleine-Weber, H.; Schroeder, S.; Kruger, N.; Herrler, T.; Erichsen, S.; Schiergens, T. S.; Herrler, G.; Wu, N. H.; Nitsche, A.; et al. SARS-CoV-2 Cell Entry Depends on ACE2 and TMPRSS2 and Is Blocked by a Clinically Proven Protease Inhibitor. *Cell* **2020**, *181*, 271−280 e278.
(5) Vaduganathan, M.; Vardeny, O.; Michel, T.; McMurray, J. J. V.; Pfeffer, M. A.; Solomon, S. D. Renin-Angiotensin-Aldosterone System Inhibitors in Patients with Covid-19. *N. Engl. J. Med.* **2020**, *382*, 1653−1659.
(6) Li, W.; Moore, M. J.; Vasilieva, N.; Sui, J.; Wong, S. K.; Berne, M. A.; Somasundaran, M.; Sullivan, J. L.; Luzuriaga, K.; Greenough, T. C.; et al. Angiotensin-converting enzyme 2 is a functional receptor for the SARS coronavirus. *Nature* **2003**, *426*, 450−454.
(7) Li, F. Receptor recognition mechanisms of coronaviruses: a decade of structural studies. *J. Virol.* **2015**, *89*, 1954−1964.
(8) Li, F. Structure, Function, and Evolution of Coronavirus Spike Proteins. *Annu. Rev. Virol.* **2016**, *3*, 237−261.
(9) Li, F. Structural analysis of major species barriers between humans and palm civets for severe acute respiratory syndrome coronavirus infections. *J. Virol.* **2008**, *82*, 6984−6991.
(10) Li, F.; Li, W.; Farzan, M.; Harrison, S. C. Structure of SARS coronavirus spike receptor-binding domain complexed with receptor. *Science* **2005**, *309*, 1864−1868.
(11) Wu, K.; Peng, G.; Wilken, M.; Geraghty, R. J.; Li, F. Mechanisms of host receptor adaptation by severe acute respiratory syndrome coronavirus. *J. Biol. Chem.* **2012**, *287*, 8904−8911.
(12) Xu, C.; Wang, Y.; Liu, C.; Zhang, C.; Han, W.; Hong, X.; Wang, Y.; Hong, Q.; Wang, S.; Zhao, Q.; et al. Conformational dynamics of SARS-CoV-2 trimeric spike glycoprotein in complex with receptor ACE2 revealed by cryo-EM. *Sci. Adv.* **2021**, *7*, No. eabe5575.
(13) Walls, A. C.; Park, Y. J.; Tortorici, M. A.; Wall, A.; McGuire, A. T.; Veesler, D. Structure, Function, and Antigenicity of the SARS-CoV-2 Spike Glycoprotein. *Cell* **2020**, *181*, 281−292 e286.
(14) Kirchdoerfer, R. N.; Wang, N.; Pallesen, J.; Wrapp, D.; Turner, H. L.; Cottrell, C. A.; Corbett, K. S.; Graham, B. S.; McLellan, J. S.; Ward, A. B. Stabilized coronavirus spikes are resistant to conformational changes induced by receptor recognition or proteolysis. *Sci. Rep.* **2018**, *8*, No. 15701.
(15) Li, W.; Zhang, C.; Sui, J.; Kuhn, J. H.; Moore, M. J.; Luo, S.; Wong, S. K.; Huang, I. C.; Xu, K.; Vasilieva, N.; et al. Receptor and viral determinants of SARS-coronavirus adaptation to human ACE2. *EMBO J.* **2005**, *24*, 1634−1643.
(16) Sui, J.; Li, W.; Murakami, A.; Tamin, A.; Matthews, L. J.; Wong, S. K.; Moore, M. J.; Tallarico, A. S.; Olurinde, M.; Choe, H.; et al. Potent neutralization of severe acute respiratory syndrome (SARS) coronavirus by a human mAb to S1 protein that blocks receptor association. *Proc. Natl. Acad. Sci. U.S.A.* **2004**, *101*, 2536−2541.
(17) Walls, A. C.; Xiong, X.; Park, Y. J.; Tortorici, M. A.; Snijder, J.; Quispe, J.; Cameroni, E.; Gopal, R.; Dai, M.; Lanzavecchia, A.; et al. Unexpected Receptor Functional Mimicry Elucidates Activation of Coronavirus Fusion. *Cell* **2019**, *176*, 1026−1039 e1015.
(18) Wong, S. K.; Li, W.; Moore, M. J.; Choe, H.; Farzan, M. A 193-amino acid fragment of the SARS coronavirus S protein efficiently binds angiotensin-converting enzyme 2. *J. Biol. Chem.* **2004**, *279*, 3197−3201.
(19) Wan, Y.; Shang, J.; Graham, R.; Baric, R. S.; Li, F. Receptor Recognition by the Novel Coronavirus from Wuhan: an Analysis Based on Decade-Long Structural Studies of SARS Coronavirus. *J. Virol.* **2020**, *94*, No. e00127-20.
(20) Holshue, M. L.; DeBolt, C.; Lindquist, S.; Lofy, K. H.; Wiesman, J.; Bruce, H.; Spitters, C.; Ericson, K.; Wilkerson, S.; Tural, A.; et al. First Case of 2019 Novel Coronavirus in the United States. *N. Engl. J. Med.* **2020**, *382*, 929−936.
(21) Liang, C.; Tian, L.; Liu, Y.; Hui, N.; Qiao, G.; Li, H.; Shi, Z.; Tang, Y.; Zhang, D.; Xie, X.; Zhao, X. A promising antiviral candidate drug for the COVID-19 pandemic: A mini-review of remdesivir. *Eur. J. Med. Chem.* **2020**, *201*, No. 112527.
(22) Wang, M.; Cao, R.; Zhang, L.; Yang, X.; Liu, J.; Xu, M.; Shi, Z.; Hu, Z.; Zhong, W.; Xiao, G. Remdesivir and chloroquine effectively inhibit the recently emerged novel coronavirus (2019-nCoV) in vitro. *Cell Res.* **2020**, *30*, 269−271.
(23) Lu, H. Drug treatment options for the 2019-new coronavirus (2019-nCoV). *Biosci. Trends* **2020**, *14*, 69−71.
(24) Zhu, Z.; Lu, Z.; Xu, T.; Chen, C.; Yang, G.; Zha, T.; Lu, J.; Xue, Y. Arbidol monotherapy is superior to lopinavir/ritonavir in treating COVID-19. *J. Infect.* **2020**, *81*, e21−e23.
(25) Spezzani, V.; Piunno, A.; Iselin, H. U. Benign COVID-19 in an immunocompromised cancer patient—the case of a married couple. *Swiss Med. Wkly.* **2020**, *150*, No. w20246.
(26) Furuta, Y.; Takahashi, K.; Shiraki, K.; Sakamoto, K.; Smee, D. F.; Barnard, D. L.; Gowen, B. B.; Julander, J. G.; Morrey, J. D. T-705 (favipiravir) and related compounds: Novel broad-spectrum inhibitors of RNA viral infections. *Antiviral Res.* **2009**, *82*, 95−102.
(27) Ferron, F.; Subissi, L.; Silveira De Morais, A. T.; Le, N. T. T.; Sevajol, M.; Gluais, L.; Decroly, E.; Vonrhein, C.; Bricogne, G.; Canard, B.; Imbert, I. Structural and molecular basis of mismatch correction and ribavirin excision from coronavirus RNA. *Proc. Natl. Acad. Sci. U.S.A.* **2018**, *115*, E162−E171.
(28) Krajczyk, A.; Kulinska, K.; Kulinski, T.; Hurst, B. L.; Day, C. W.; Smee, D. F.; Ostrowski, T.; Januszczyk, P.; Zeidler, J. Antivirally active ribavirin analogues–4,5-disubstituted 1,2,3-triazole nucleosides: biological evaluation against certain respiratory viruses and computational modelling. *Antiviral Chem. Chemother.* **2014**, *23*, 161−171.
(29) Pepperrell, T.; Pilkington, V.; Owen, A.; Wang, J.; Hill, A. M. Review of safety and minimum pricing of nitazoxanide for potential treatment of COVID-19. *J. Virus Erad.* **2020**, *6*, 52−60.
(30) Tilmanis, D.; van Baalen, C.; Oh, D. Y.; Rossignol, J. F.; Hurt, A. C. The susceptibility of circulating human influenza viruses to tizoxanide, the active metabolite of nitazoxanide. *Antiviral Res.* **2017**, *147*, 142−148.
(31) Fantini, J.; Di Scala, C.; Chahinian, H.; Yahi, N. Structural and molecular modelling studies reveal a new mechanism of action of chloroquine and hydroxychloroquine against SARS-CoV-2 infection. *Int. J. Antimicrob. Agents* **2020**, *55*, No. 105960.
(32) Hall, D. C., Jr.; Ji, H. F. A search for medications to treat COVID-19 via in silico molecular docking models of the SARS-CoV-2

https://doi.org/10.1021/acsomega.2c00844
ACS Omega 2022, 7, 28779−28789

spike glycoprotein and 3CL protease. *Travel Med. Infect. Dis.* **2020**, *35*, No. 101646.
(33) Sun, C.; Zhang, J.; Wei, J.; Zheng, X.; Zhao, X.; Fang, Z.; Xu, D.; Yuan, H.; Liu, Y. Screening, simulation, and optimization design of small molecule inhibitors of the SARS-CoV-2 spike glycoprotein. *PLoS One* **2021**, *16*, No. e0245975.
(34) Chen, C. Z.; Xu, M.; Pradhan, M.; Gorshkov, K.; Petersen, J. D.; Straus, M. R.; Zhu, W.; Shinn, P.; Guo, H.; Shen, M.; Klumpp-Thomas, C.; Michael, S. G.; Zimmerberg, J.; Zheng, W.; Whittaker, G. R. Identifying SARS-CoV-2 Entry Inhibitors through Drug Repurposing Screens of SARS-S and MERS-S Pseudotyped Particles. *ACS Pharmacol. Transl. Sci.* **2020**, *3*, 1165−1175.
(35) Sun, H.; Wang, Y.; Chen, C. Z.; Xu, M.; Guo, H.; Itkin, M.; Zheng, W.; Shen, M. Identification of SARS-CoV-2 viral entry inhibitors using machine learning and cell-based pseudotyped particle assay. *Bioorg. Med. Chem.* **2021**, *38*, No. 116119.
(36) Hu, X.; Chen, C. Z.; Xu, M.; Hu, Z.; Guo, H.; Itkin, Z.; Shinn, P.; Ivin, P.; Leek, M.; Liang, T. J.; Shen, M.; Zheng, W.; Hall, M. D. Discovery of Small Molecule Entry Inhibitors Targeting the Fusion Peptide of SARS-CoV-2 Spike Protein. *ACS Med. Chem. Lett.* **2021**, *12*, 1267−1274.
(37) Acharya, A.; Pandey, K.; Thurman, M.; Klug, E.; Trivedi, J.; Sharma, K.; Lorson, C. L.; Singh, K.; Byrareddy, S. N. Discovery and Evaluation of Entry Inhibitors for SARS-CoV-2 and Its Emerging Variants. *J. Virol.* **2021**, *95*, No. e0143721.
(38) Wang, L.; Wu, Y.; Yao, S.; Ge, H.; Zhu, Y.; Chen, K.; Chen, W. Z.; Zhang, Y.; Zhu, W.; Wang, H. Y.; Guo, Y.; Ma, P. X.; Ren, P. X.; Zhang, X. L.; Li, H. Q.; Ali, M. A.; Xu, W. Q.; Jiang, H. L.; Zhang, L. K.; Zhu, L. L.; Ye, Y.; Shang, W. J.; Bai, F. Discovery of potential small molecular SARS-CoV-2 entry blockers targeting the spike protein. *Acta Pharmacol. Sin.* **2021**, *43*, 788−796.
(39) Xiong, J.; Xiang, Y.; Huang, Z.; Liu, X.; Wang, M.; Ge, G.; Chen, H.; Xu, J.; Zheng, M.; Chen, L. Structure-Based Virtual Screening and Identification of Potential Inhibitors of SARS-CoV-2 S-RBD and ACE2 Interaction. *Front. Chem.* **2021**, *9*, No. 740702.
(40) Sheahan, T. P.; Sims, A. C.; Zhou, S.; Graham, R. L.; Pruijssers, A. J.; Agostini, M. L.; Leist, S. R.; Schafer, A.; Dinnon, K. H., 3rd; Stevens, L. J.; et al. An orally bioavailable broad-spectrum antiviral inhibits SARS-CoV-2 in human airway epithelial cell cultures and multiple coronaviruses in mice. *Sci Transl. Med.* **2020**, *12*, No. S0883.
(41) Mahase, E. Covid-19: Pfizer's paxlovid is 89% effective in patients at risk of serious illness, company reports. *BMJ* **2021**, *375*, No. n2713.
(42) Humphrey, W.; Dalke, A.; Schulten, K. VMD: visual molecular dynamics. *J. Mol. Graphics* **1996**, *14*, 33−38.
(43) *Computer-Aided Molecular Design*; MOE Chemical Computing Group: Montreal, Quebec, Canada, 2022. http://www.chemcomp.com.
(44) *eMolecules*; eMolecules, Inc: La Jolla, CA, 2022. http://www.emolecules.com/.
(45) *FRED, vROCS, OMEGA and VIDA*; OpenEye Scientific Software: Santa Fe, NM, 2022. http://www.eyesopen.com/.
(46) *The PyMOL Molecular Graphics System*, version 1.8.2.3; Schrödinger, LLC, 2022.
(47) Jawad, B.; Adhikari, P.; Podgornik, R.; Ching, W. Key Interacting Residues between RBD of SARS-CoV-2 and ACE2 Receptor: Combination of Molecular Dynamics Simulation and Density Functional Calculation. *J. Chem. Inf. Model.* **2021**, *61*, 4425−4441.
(48) Ali, A.; Vijayan, R. Dynamics of the ACE2-SARS-CoV-2/SARS-CoV spike protein interface reveal unique mechanisms. *Sci. Rep.* **2020**, *10*, No. 14214.
(49) Ngo, V. A.; Jha, R. K. Identifying key determinants and dynamics of SARS-CoV-2/ACE2 tight interaction. *PLoS One* **2021**, *16*, No. e0257905.
(50) ClinicalTrials.gov. Carrageenan Nasal Spray for COVID-19 Prophylaxis (ICE-COVID). https://clinicaltrials.gov/ct2/show/NCT04590365 (accessed Feb 5, 2022).
(51) Andrew, M.; Jayaraman, G. Marine sulfated polysaccharides as potential antiviral drug candidates to treat Corona Virus disease (COVID-19. *Carbohydr. Res.* **2021**, *505*, No. 108326.
(52) Lau, E. Y.; Negrete, O. A.; Bennett, W. F. D.; Bennion, B. J.; Borucki, M.; Bourguet, F.; Epstein, A.; Franco, M.; Harmon, B.; He, S.; Jones, D.; Kim, H.; Kirshner, D.; Lao, V.; Lo, J.; McLoughlin, K.; Mosesso, R.; Murugesh, D. K.; Saada, E. A.; Segelke, B.; Stefan, M. A.; Stevenson, G. A.; Torres, M. W.; Weilhammer, D. R.; Wong, S.; Yang, Y.; Zemla, A.; Zhang, X.; Zhu, F.; Allen, J. E.; Lightstone. Discovery of Small-Molecule Inhibitors of SARS-CoV-2 Proteins Using a Computational and Experimental Pipeline. *Front. Mol. Biosci.* **2021**, *8*, No. 678701.
(53) Stevenson, G. A.; Jones, D.; Kim, H.; Bennett, WFD.; Bennion, B. J.; Borucki, M.; Bourguet, F.; Epstein, A.; Franco, M.; Harmon, B.; He, S.; Katz, M. P.; Kirshner, D.; Lao, V.; Lau, E. Y.; Lo, J.; McLoughlin, K.; Mosesso, R.; Murugesh, D. K.; Negrete, O. A.; Saada, E. A.; Segelke, B.; Stefan, M.; Torres, M. W.; Weilhammer, D.; Wong, S.; Yang, Y.; Zemla, A.; Zhang, X.; Zhu, F.; Lightstone, F. C.; Allen, J. E. High-Throughput Virtual Screening of Small Molecule Inhibitors for SARS-CoV-2 Protein Targets with Deep Fusion Models, 2021. http://arxiv.org/abs/physics/2104.04547.
(54) Schmidt, F.; Weisblum, Y.; Rutkowska, M.; et al. High genetic barrier to SARS-CoV-2 polyclonal neutralizing antibody escape. *Nature* **2021**, *600*, 512−516.
(55) Piccoli, L.; Park, Y. J.; Tortorici, M. A.; Czudnochowski, N.; Walls, A. C.; Beltramello, M.; Silacci-Fregni, C.; Pinto, D.; Rosen, L. E.; et al. Mapping Neutralizing and Immunodominant Sites on the SARS-CoV-2 Spike Receptor-Binding Domain by Structure-Guided High-Resolution Serology. *Cell* **2020**, *183*, 1024−1042.
(56) Schmidt, F.; Weisblum, Y.; Muecksch, F.; Hoffmann, H. H.; Michailidis, E.; Lorenzi, J. C. C.; Mendoza, P.; Rutkowska, M.; Bednarski, E.; Gaebler, C.; et al. Measuring SARS-CoV-2 neutralizing antibody activity using pseudotyped and chimeric viruses. *J. Exp. Med.* **2020**, *217*, No. e20201181.
(57) Alsaidi, S.; Cornejal, N.; Mahoney, O.; Melo, C.; Verma, N.; Bonnaire, T.; Chang, T.; O'Keefe, B. R.; Sailer, J.; Zydowsky, T. M.; et al. Griffithsin and Carrageenan Combination Results in Antiviral Synergy against SARS-CoV-1 and 2 in a Pseudoviral Model. *Mar Drugs* **2021**, *19*, No. 418.

https://doi.org/10.1021/acsomega.2c00844
ACS Omega 2022, 7, 28779−28789